ELSEVIER

Materials Science and Engineering A 420 (2006) 306–314

MATERIALS SCIENCE & ENGINEERING A

www.elsevier.com/locate/msea

Dynamic recrystallization of Ni-base alloys—Experimental results and comparisons with simulations

P. Poelt [a,*], C. Sommitsch [b], S. Mitsche [a], M. Walter [c]

[a] *Institute for Electron Microscopy, Graz University of Technology, Steyrerg 17, A-8010 Graz, Austria*
[b] *Chair of Metal Forming, University of Leoben, Franz-Josef-Str. 18, A-8700 Leoben, Austria*
[c] *Böhler Edelstahl GmbH, POB 96, A-8605 Kapfenberg, Austria*

Received 20 April 2005; received in revised form 13 January 2006; accepted 16 January 2006

Abstract

The dynamic recrystallization of the Ni-base alloy Böhler L306 VMR (Alloy 80A) in a transient state was investigated both by light microscopy and electron backscatter diffraction (EBSD), and the experimental results were compared with those from simulations. Subgrain structures of the size of the recrystallized grains were observed close to the grain boundaries of the original grains. With increasing strain a texture developed in the deformed fraction. Strong twinning was found in the recrystallized fraction, with area fractions of the twinned grains of around 80% for higher strains. Thus the measured grain sizes strongly depend on the handling of the twins. A pronounced increase in the average grain size of the recrystallized fraction with increasing strain (time) was only observed after twin removal. There was generally good agreement between the measured and the simulated results.

Keywords: Dynamic recrystallization; Nickel-base alloy; Electron backscatter diffraction; Modeling

1. Introduction

Hot forming of metals and alloys involves recrystallization, which is often used to tune the properties of the respective material. The recrystallization process mainly influences the microstructure and the mechanical properties and thus the formability of the materials, whereas the physical properties such as electrical resistivity undergo much smaller changes [1,2]. Dynamic recrystallization comprises, besides other elementary mechanisms, grain boundary migration and the evolution of subgrain boundaries to high angle boundaries. Depending on which of these two processes is prevalent, either grain coarsening or grain refinement occurs [3,4].

Parameters like the size, the distribution and the volume fraction of both the recrystallized grains and deformed grains and possible textures influence the behavior of the material. Electron back scatter diffraction (EBSD) in the scanning electron microscope (SEM) has emerged as a very useful tool for the measurement of these parameters because of its ability to differentiate between different types of grains and to elucidate direct neighborhood relationships between individual grains [5,6]. These relationships can provide information about which types of grain boundaries recrystallization preferentially starts at and also on the effects of twinning.

However, EBSD also suffers from one major disadvantage: it is relatively time consuming and therefore, depending on the grain size, the measurements generally comprise only between several hundred and several thousand grains with the consequence of poor statistical results. Thus the more conventional technique of specimen etching and optical microscopy (LIMI) might still be a very useful tool, especially as far as grain size distributions are concerned.

Whereas EBSD provides information about the structure of a material at a certain stage of the recrystallization process, it does not give any direct insight into the underlying physical principles governing the evolution process. This is the point where simulations come in. It is the comparison between the simulated and the measured results that should pave the way for the choice of the appropriate model for the description of the microstructural evolution.

Additionally, simulations allow the prediction of material properties in connection with experimental parameters not

* Corresponding author. Tel.: +43 316 873 8321; fax: +43 316 811596.
E-mail address: peter.poelt@felmi-zfe.at (P. Poelt).

0921-5093/$ – see front matter © 2006 Elsevier B.V. All rights reserved.
doi:10.1016/j.msea.2006.01.076

Table 1
Chemical composition (wt.%) of the Alloy 80A (Böhler L306)

C	Al	Si	Ti	Cr	Mn	Co	Ni	Mo
0.06	1.67	0.15	2.52	19.60	0.04	0.06	75.10	0.03

directly accessible with the equipment available. The model here finds practical use in the optimization of hot forming of nickel-base superalloys. In order to ensure the mechanical properties demanded from the rolled and forged products, a homogeneous and completely recrystallized structure must be achieved. The corresponding processing can be improved substantially by the numerical simulation of the structure development, coupled with finite element analysis (FEA), in particular with regard to relatively small forming windows as well as to large gradients of temperature and deformation rate in large sized blooms. In distinction to semi-empirical models, the approach presented here can consider both recrystallization cycles and the interaction of recrystallization and precipitations. However, modeling of precipitation will not be considered explicitly in this work. In addition, the grain size distribution can be computed and the flow stress is calculated as a function of the mean dislocation density as an input parameter for the FEA. The model was tested for the Ni-base grades Alloy 80A as well as Alloy 718 for typical hot forming conditions for open die forging and radial forging ($950\,^{\circ}\mathrm{C} < T < 1200\,^{\circ}\mathrm{C}$, $0.01 < \dot{\varepsilon} < 10\,\mathrm{s}^{-1}$).

2. Experimental techniques

2.1. Gleeble tests

Samples of Böhler L306 VMR (Alloy 80A, chemical composition see Table 1) were cut from hot rolled pieces, thus ensuring a completely recrystallized, fine-grained and homogeneous microstructure. After a solution heat treatment at 1220 °C for 60 s, hot compression tests were carried out on a Gleeble 3800 testing system. The short annealing time was chosen to avoid grain growth, leading to an initial grain size of around 120 μm. The cylindrical compression samples ($h = 12$ mm, $d = 10$ mm) were cooled down to the test temperature of 1120 °C and subsequently compressed at a constant strain rate of $0.1\,\mathrm{s}^{-1}$ to different strains. Finally the compressed specimens were cut to both longitudinal (specimen center) and transversal cross sections for microstructural observations. The latter sections were chosen at a quarter of the specimen height. Finite element calculations of the compression tests proved that the local and the global strain rates correspond in this section from the center to half of the radius. Fig. 1 shows the stress–strain curve for $T = 1120\,^{\circ}\mathrm{C}$ and $\dot{\varepsilon} = 0.1\,\mathrm{s}^{-1}$.

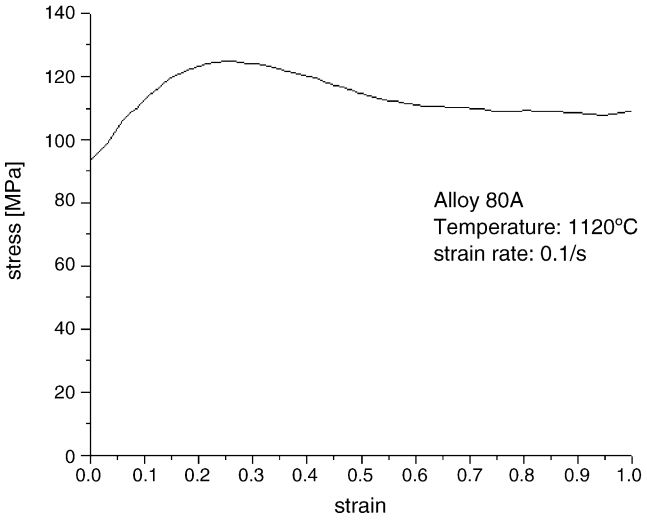

Fig. 1. Stress–strain curve for $T = 1120\,^{\circ}\mathrm{C}$ and $\dot{\varepsilon} = 0.1\,\mathrm{s}^{-1}$.

2.2. Etching of specimens, optical microscopy

The specimens were embedded in epoxy resin and polished. An electrolyte based on glycerine and hydrofluoric acid, which suppresses etching of the twin boundaries, was used for subsequent electrolytic etching. It also gives a very uniform etching of the grain boundaries and thus facilitates the grain boundary reconstruction and evaluation, performed by the image processing system ImageC© from Aquinto and controlled by a home-made script (Fig. 2). The differentiation between the recrystallized grains and the deformed grains was based on the ratio of the diameter of a coextensive circle to the diameter of a circle with the same perimeter length as that of the respective grain [7]. This ratio is relatively close to the ideal ratio of a circular area for the recrystallized grains. On the other hand, with increasing progress in the recrystallization process the original grains develop a rather frayed boundary structure. The corresponding ratio decreases considerably as a consequence. An appropriate threshold value of 0.125 was established, and grains exceeding this threshold counted as recrystallized grains. But less deformed grains cut close to the edges may corrupt the results.

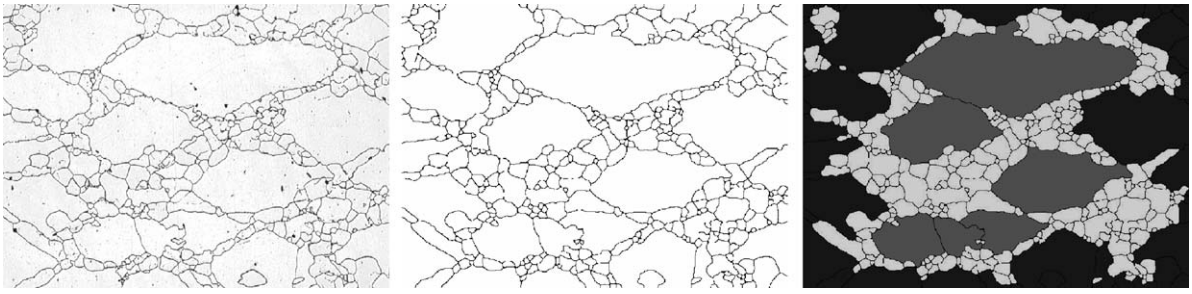

Fig. 2. LIMI images, from left to right: after etching, after thresholding, as evaluated.

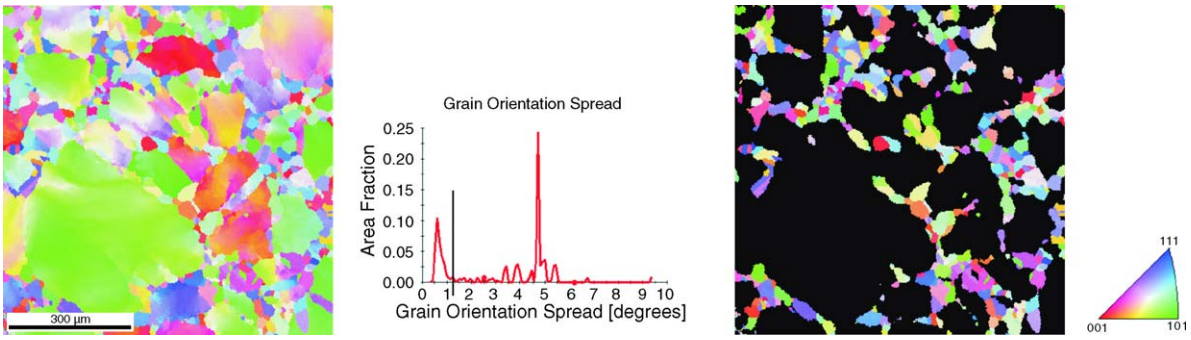

Fig. 3. EBSD measurements, from left to right: inverse pole figure (IPF) map of the whole scanned area (image width: 809 μm); grain orientation spread, with the vertical line marking the critical spread for the discrimination between the recrystallized and the deformed fraction; IPF map of the recrystallized fraction only, with the black area marking the deformed fraction; color code for the IPF maps.

2.3. Electron backscatter diffraction

The EBSD measurements and analyses were performed using a TSL system (SIT camera, OIM^{TM} 4 software) attached to a Zeiss Gemini 982 DSM (primary electron energy: 20 keV; probe current: 2.8 nA). Colloidal silica was used for the final polishing of the specimens. To minimize the influence of noise in the results, a grain must comprise at least six pixel, resulting in a minimum grain diameter of around 7 μm. Grain boundaries were characterized by a misorientation >5° between neighboring measurement points.

Several methods were tried for the discrimination between the still deformed and the recrystallized grains, but the grain orientation spread proved to be most successful [8–10]. A typical example with the two fractions separated can be found in Fig. 3. The first peak in the grain orientation spread chart belongs predominantly to the recrystallized fraction. The orientation spread value for the partitioning of the two fractions was generally between 1.2° and 1.8°. The accuracy of the orientation measurements with the EBSD system was tested using a tempered Ni-base specimen of Alloy 80 as standard, where almost no misorientation spread should be present within the grains. The measured spread had a peak at around 0.3° and a half width of around 0.2°. Thus the error in the measurements should be less than 0.5°.

3. Simulation

3.1. Criteria for dynamic recrystallization

During hot forming, the mean dislocation density rate can be described by the equation [11]

$$\frac{d\rho_0}{dt} = \frac{\dot{\varepsilon}}{bl_0} - 2M\tau\rho_0^2, \quad (1)$$

taking the strain hardening and the recovery of dislocations into account, but neglecting recrystallization, where $\dot{\varepsilon}$ is the strain rate, b the Burgers vector, l_0 the mean free path of the dislocations ($l_0 \sim \rho_0^{-1/2}$), M the mobility of recovery and τ is the average energy per unit length of a dislocation.

A critical dislocation density is necessary in order to initiate dynamic recrystallization. The nucleus usually forms at pre-existing grain boundaries in the material, at least at higher strain rates. For an area that has just been recrystallized it is assumed that the dislocation density ρ_0 generated by the preceding strain is reduced to a very low value. Roberts and Ahlblom [12] developed a nucleation criterion, which is based upon the idea that during dynamic recrystallization the concurrent deformation reduces the stored energy difference (driving force) that effects migration of a high angle boundary. The nucleation theory gives the net free energy change.

Maximizing the net free energy change produces the critical nucleation conditions, which are the critical radius r_{cr} of a recrystallization nucleus and the critical dislocation density ρ_{cr} for the onset of recrystallization.

3.2. Nucleation model

Dynamic recrystallization can be considered in terms of the rate of nucleation (formation of interfaces) versus the rate of growth (migration of interfaces) under given boundary conditions. A model that considers the dynamic balance of these two rates was proposed by Srinivasan and Prasad [13]. The nucleation consists of the formation of a grain boundary due to dislocation generation, and simultaneous recovery and rearrangement. This interface will become a nucleus for dynamic recrystallization when it attains a critical configuration, i.e. that of a high angle boundary. The nucleus will grow by the process of grain boundary migration. Since under hot working conditions the material acts essentially as a dissipator of power, the driving force for the migration of interfaces is the reduction of total interface energy. When nucleation and growth occur simultaneously, the slower of the two will control dynamic recrystallization.

The rate of annihilation of recovered groups of dislocations (interfaces) as a result of interface migration depends upon the mobility of the boundary. On the other hand, the rate of interface formation depends on the rate of generation of recovered dislocations. In [13], it has been shown that for nickel the rate of nucleation is lower than the rate of growth by about four orders of magnitude and therefore controls the dynamic recrystallization process. For nickel and nickel-based superalloys with their relatively low stacking fault energies at high temperatures, mechanical recovery involving cross slip of screw dislocations can be neglected in comparison with thermal recovery based on

climb of edge dislocations. Hence the rate of interface formation R_F for these types of alloys can be described by [14]

$$R_F = \frac{\dot{\varepsilon} P_R}{b l_0}, \tag{2}$$

where P_R is the probability of recovery of dislocations.

Let $N_d = A_{cr}/l_{cr}^2$ be the number of dislocations per critical nucleus, A_{cr} the cross section of a critical nucleus and l_{cr} the mean free path of dislocations with a critical density ($l_{cr} \sim \rho^{-1/2}$), where N_d, A_{cr} as well as l_{cr} are time dependent, if the deformation variables temperature and strain rate change with time. Therefore, R_F/N_d is the number of nuclei generated per unit area and unit time. If we assume that nuclei preferentially form at high angle grain boundaries of the deformed grains with mean diameter D_0, the grain boundary area per unit volume is proportional to the reciprocal of $D_0[D_0^2/D_0^3 = 1/D_0]$ and therefore $[R_F/(N_d D_0)]$ is proportional to the number of nuclei generated per unit volume and unit time. Therefore the number of nuclei N per volume can be calculated by

$$N(t) = \int_{t_{cr}}^{t_b} R_N(t)\,dt = \int_{t_{cr}}^{t_b} \frac{R_F(t)}{N_d(t) D_0}[1 - f(t)]\,dt, \tag{3}$$

where R_N is the nucleation rate per unit volume, t_{cr} is the time when the critical dislocation density is exceeded and t_b is the time of observation.

3.3. Recrystallization model

The following model is described in detail in Sommitsch et al. [14,15]. The recrystallized fraction $f(t_b)$ at time t_b is given by the sum over all nucleation times t_g, starting at time t_{cr}, where the dislocation density reaches the critical value ($\rho_0 \geq \rho_{cr}$):

$$f(t_b) = \frac{\pi}{6} \int_{t_{cr}}^{t_b} D^3(t_g, t_b) R_N(t_g)[1 - f(t_g)]\,dt_g, \tag{4}$$

where $R_N(t_g)\,dt_g$ grains are nucleated in the time interval $[t_g, t_g + dt_g]$ and $D(t_g, t_b)$ is the size of a recrystallized grain nucleated at time t_g:

$$D(t_g, t_b) = D_{cr}(t_g) + 2 \int_{t_g}^{t_b} v(\tau)\,d\tau, \tag{5}$$

with $D_{cr} = 2r_{cr}$ and t_g as the time of generation of a new grain class. The grain boundary velocity v depends on time due to the precipitation of particles, changing temperature and strain rate. Hence the velocity of a high angle boundary during recrystallization is the product of the boundary mobility m, the sum of the driving and dragging forces and a diminishing factor K_S, therefore,

$$v = m(\tau \Delta\rho - P_Z) K_S, \tag{6}$$

where P_Z is the Zener drag [16] and K_S is a factor that represents the solute drag for high boundary velocities [17]. $\tau\Delta\rho$ denotes the stored energy difference ($\Delta\rho \approx \rho_0$) in the vicinity of the boundary, with ρ_0 as the mean dislocation density in the deformed grains.

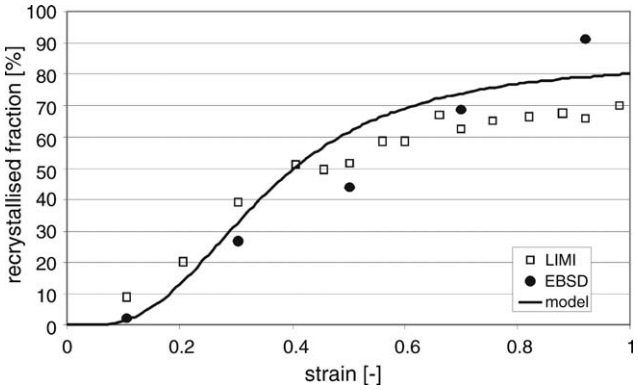

Fig. 4. Comparison of the measured (EBSD and LIMI) and calculated recrystallized fraction as a function of the strain.

In the model presented here, a second recrystallization cycle is initiated if the mean dislocation density of recrystallized grains of the first cycle exceeds the critical dislocation density. The nucleation rate of the second cycle is thus related to the mean recrystallized grain size and the dislocation density of the first cycle. The formulation of a third cycle has not yet been implemented into the model, hence the calculated evolution of dynamic recrystallization is restricted to two cycles, which is not necessarily sufficient, however, for reaching a steady state during dynamic recrystallization.

4. Results

4.1. Determination of the recrystallized fraction

A sound interpretation of the measured results is only possible if a reliable procedure for the differentiation between the deformed and the recrystallized grains is available. Inherent in both methods explained above is a parameter – a critical perimeter to area ratio for LIMI measurements and a critical grain orientation spread for EBSD measurements – that is not well-defined and not enforced by a basic principle, but can be chosen within certain limits. The comparison between the two experimental methods and the simulation in Fig. 4 demonstrate that at low strains the results gained by LIMI match very well with those measured by EBSD and are also close to the calculated values. Generally, rather higher values would be expected for LIMI compared to EBSD. This is due to the fact that the imaging system is not always able to relate profiles from big deformed grains, which are cut close to the edges (corresponding to a section close to the pole for a sphere) and thus are comparable in size to the recrystallized grains, to the deformed fraction. But a careful choice of the threshold value can apparently minimize this error at least for low strains.

On the contrary, there is a strong deviation between the LIMI and the EBSD results for high strains. Whereas the recrystallized fraction measured by EBSD increases with increasing strain, with a value already >90% for a strain of 0.92, the LIMI values stay approximately constant at a value of around 60–70% for the recrystallized fraction. A similar behavior is also shown by results from the simulations.

There are several reasons why both methods could give wrong results for high strains. With increasing strain, the grains that recrystallized very early during the compression test are deformed concomitantly, thus making it difficult for EBSD to discriminate between the initially deformed grains and the recrystallized ones. Even recrystallization of some overcritically strained grains of the already recrystallized fraction could take place. The extreme twinning observed and the ongoing growth of the recrystallized grains with increasing strain, with a preference for growth in the direction of the grain boundaries, could also change their average perimeter to area ratio to values closer to that of the deformed grains and thus distort the LIMI results.

However, the initially very large average diameter of the deformed grains approaches the grain size of the recrystallized fraction (see below) at higher strains and thus is an indication that finally all the deformed grains will be consumed, making the EBSD results more reliable.

Fig. 5 proves that the calculated values for the nucleus density match closely with the experimental results. As the model calculations do not include a separate consideration of twins besides large angle grain boundaries, they have to be compared with the corresponding set of EBSD measurements (all twins removed in Fig. 5). The differences between the EBSD and the LIMI results might be caused by the same effects as those given for the differences in the recrystallized fraction.

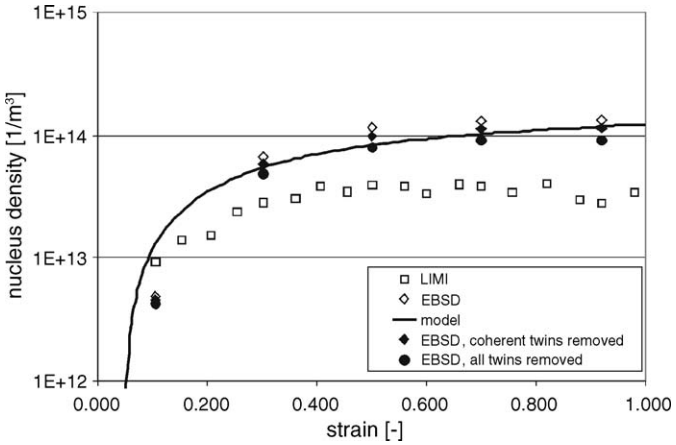

Fig. 5. Comparison of the measured (EBSD and LIMI) and calculated nucleus density as a function of the strain.

4.2. Evolution of the recrystallized fraction

Fig. 6 shows the evolution of the recrystallized fraction with strain for one set of measurements. It demonstrates that recrystallization predominantly starts at edge points of grains. Although recrystallization commences, of course, with the formation of single isolated grains, these grains do not remain isolated, but represent nuclei for further recrystallization along some preferential grain boundaries, very soon forming closed networks and resulting in the well-known necklace structure. Thus, the

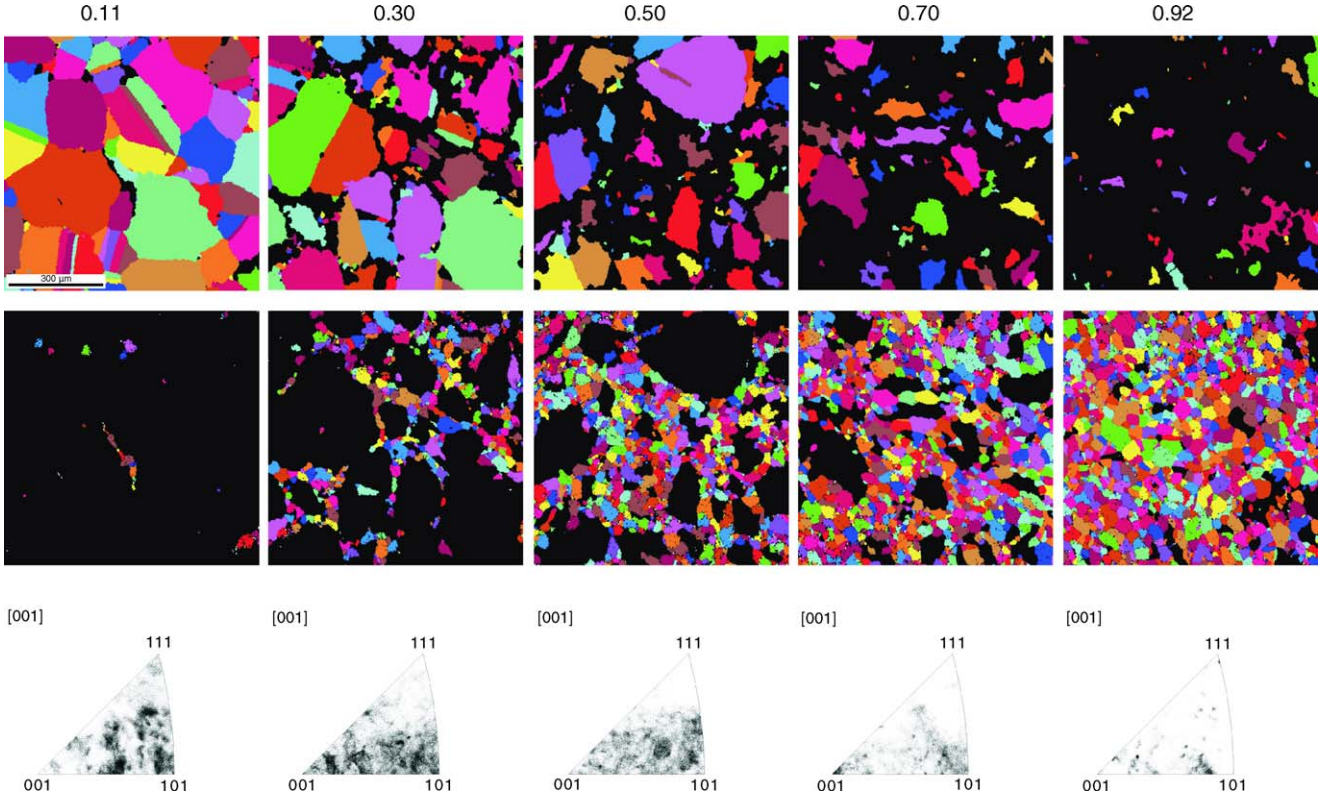

Fig. 6. EBSD measurements: grain maps (image width: 809 μm) of the deformed (top) and recrystallized (center) fraction and the inverse pole figures of the deformed fraction as function of the strain, with the strain values atop of the image. The black areas represent the corresponding second fraction. The coherent twins have been removed.

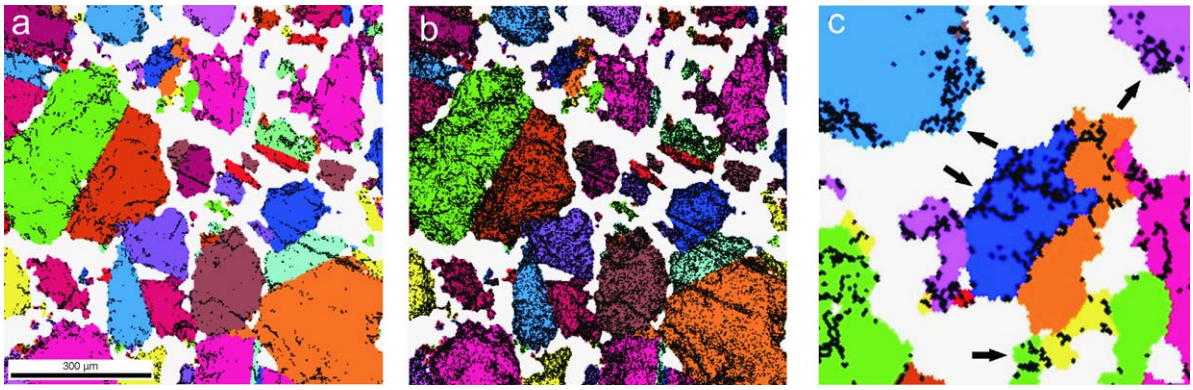

Fig. 7. EBSD measurements: grain maps of the deformed fraction at a strain of 0.3, with the bold black dots marking small angle misorientations >2° (a and c) and >1° (b) in the range between 1° and 5°. Fig. 9c is a section of Fig. 9a, with the arrows marking regions with small angle grain boundaries. The white areas represent the recrystallized fraction. Image width of a and b: 809 μm, of c: 215 μm.

necklace is formed by a coalescence of clusters of recrystallized grains, not by fully isolated individual grains finally becoming so dense they begin to touch each other. All recrystallized grains appear along large angle grain boundaries, none inside the grains. Additionally recrystallization seems to take place at 'normal' grain boundaries with much higher probability than at twin boundaries.

One of the mechanisms for recrystallization is the transformation of subgrain boundaries into large angle grain boundaries. The example in Fig. 7 demonstrates that in many grains the majority of small angle misorientations in the range between 1° and 5° with misorientation angles >2° (Fig. 7a) are located rather close to the grain boundaries, whereas a lower value of 1° (Fig. 7b) results in an approximately statistical scatter across the whole grains. Since misorientations are caused by strains (i.e. caused by dislocations), their height and distribution should be a rough measure for the local dislocation densities. Part of the dislocations, especially those along straight lines, may also be attributed to preparation artifacts, e.g. scratches caused by specimen polishing. For comparison, a misorientation distribution for an unstrained specimen is shown in Fig. 8.

In the deformed fraction a subgrain structure close to the high angle grain boundaries can be observed, albeit not with completely closed boundaries, but with grain sizes of approximately the size of the recrystallized grains (see structures marked by arrows in Fig. 7c). Eventually, a clustering of such structures occurs with increasing strain. Thus recrystallization, if not disrupted, would have possibly progressed preferentially at these sites. This could probably fit into a special form of localized continuous recrystallization postulated by Thomas et al. [18]. It also goes very well with the observation illustrated earlier, that the recrystallized grains very often appear as clusters already at the earliest stages of the deformation process. But grain boundary transformation is not the only mechanism that could create the concave structures visible in Fig. 7c. Nucleation and grain bulging would give rise to a similar appearance of the deformed grains. Which mechanism is occurring or at least dominates cannot be extracted from the OIM maps, but a more pronounced grain growth could be expected for the latter than for the former one. But as will be shown below, grain growth with increasing strain and thus time is relatively modest. The results in any case fit very well to models from Sakai et al. [19,20], where serrated grain boundaries are considered as the main sites for both nucleation and the formation of high local orientation or strain gradients. Sakai also argues that grain boundary sliding is essentially taking place in the regions already consisting of small recrystallized grains and that this promotes the formation of successive strands of necklace structures.

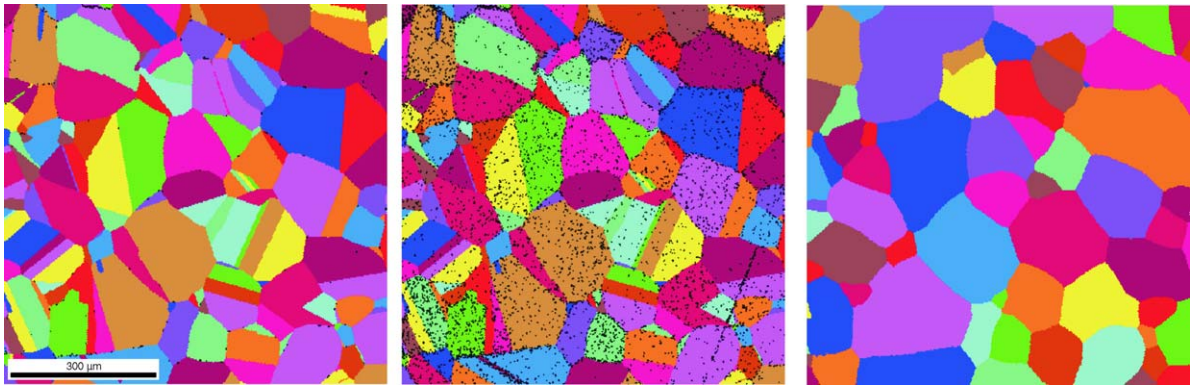

Fig. 8. EBSD measurements: grain maps (image width: 809 μm) of the unstrained material, left: bold black lines marking small angle misorientations >2°; center: small angle misorientations >1° (both in the range between 1° and 5°); right: all twin boundaries, including secondary recrystallization twins, removed (tolerance angle: 5°).

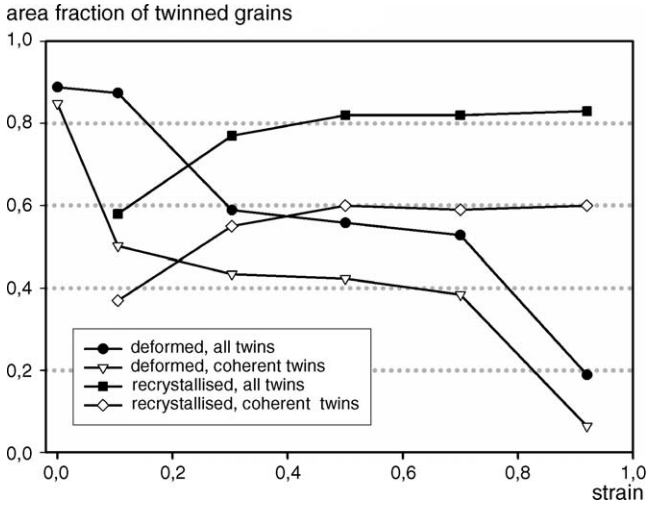

Fig. 9. EBSD measurements: area fractions of twinned grains (grains as defined in Fig. 8 right), for both the deformed and recrystallized fractions as a function of the strain. For the definition of coherent and incoherent (=all) twins see text.

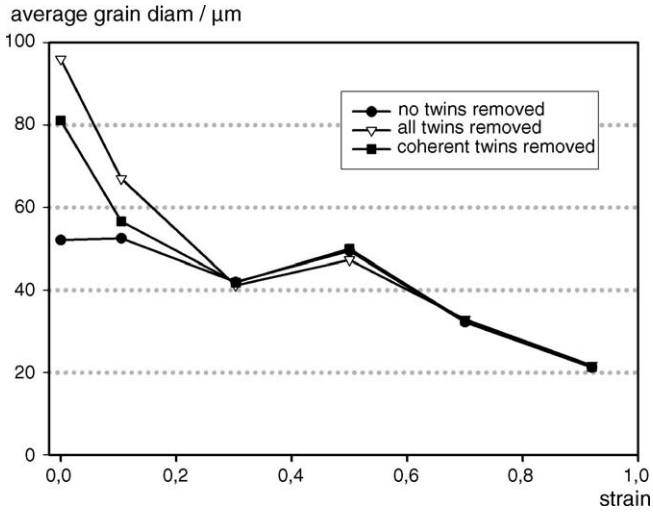

Fig. 10. EBSD measurements: average diameter of the deformed grains as a function of the strain and in dependence of twin handling. For the definition of coherent and incoherent (=all) twins see text.

The deformed fraction of the grains develops a distinct texture with increasing strain (Fig. 6). This was not observed for the recrystallized grains. The texture is caused most probably by the deformation of the material during the compression test. But in that case one would expect a similar texture for at least those grains of the recrystallized fraction formed very early during the compression. However, if their number is small enough compared to the total number of recrystallized grains, the formation of a texture could be masked. Montheillet et al. [21] state that a crystallographic texture at large strains has been observed for continuous dynamic recrystallization, whereas it was prevented in the case of discontinuous dynamic recrystallization.

A texture could also be formed if there is a preference for recrystallization along special directions. A possible reason for such an effect taking place could be that the density of the dislocations developing during straining varies for different directions.

4.3. Twinning

Although recrystallization seems rarely to take place at twin boundaries, the recrystallization process itself and the parameters by which it is governed influence the formation of twins in the recrystallized fraction. And the number of the twins and the fraction of twin boundaries endow the materials with special properties. Consequently, a differentiation between two types of grains is necessary. Firstly, the grains as obtained for example by EBSD, with no twins removed (Fig. 8, left) and providing the material with the properties desired. Secondly, the larger units obtained after twin removal (Fig. 8, right). Recrystallization mainly takes place at the boundaries of these units.

Both the grains of the unstrained material, the deformed grains at low strains and the recrystallized grains are strongly twinned (see Fig. 9), with the fraction of twinned grains dependent on whether all twins (coherent and incoherent) or only coherent twins are regarded as genuine twins. Those that meet the twinning misorientation criterion are regarded as incoherent twin boundaries, whereas for coherent twins the boundary planes have to be additionally coincident with a particular twinning plane ($\{1\,1\,1\}$ for fcc primary recrystallization twins) [1,22,23]. Since, orientation imaging microscopy maps like those in Fig. 6 are two-dimensional, they cannot provide clear information about the latter criterion. Nevertheless, the alignment of the surface traces of the twinning planes with that of the boundary planes provides some information about a possible coincidence and can be used to distinguish between coherent and incoherent twins [22,23]. The discrimination between the two different types of twins is crucial because of their different properties, e.g. unlike many types of incoherent twins, the coherent twins are nearly immobile.

For deformed grains, the fraction of twinned grains strongly decreases with increasing strain (Fig. 9). This can happen by a conversion of twin boundaries into ordinary high angle boundaries through the straining, see Thomas et al. [18]. However, it could also be explained by the fact that in a twinned pair the daughters are generally substantially smaller than the parents and thus faster consumed by recrystallization. At strains >0.5 the portion of twinned grains becomes independent of the strain and rather high for the recrystallized fraction. Thus, at least for this fraction, no substantial transformation of twin boundaries into ordinary boundaries can be observed, possibly because of the relatively low stored deformation energy within the recrystallized grains in comparison to the unrecrystallized grains. All EBSD values are averages from three sets of measurements like those shown in Fig. 6.

The calculated average grain diameters depend strongly on the comprehension of the twins (see Figs. 10 and 11). A more pronounced growth of the recrystallized grains can only be seen after twin removal, which in this case seems to be mainly caused by the formation of twins at the boundaries of recrystallizing grains. Because of the relatively small number of grains com-

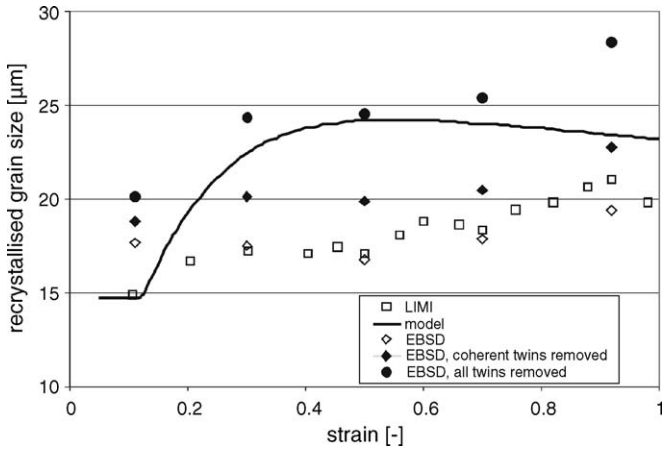

Fig. 11. Comparison of the measured (EBSD and LIMI) and calculated average grain size of the recrystallized fraction as a function of the strain. For the definition of coherent and incoherent (=all) twins see text.

prised, all graphs attributed to the deformed fraction show only tendencies, the absolute values are not really reliable. Additionally, if the crystallographic texture would be accompanied by a morphologic texture, the area fractions would not be equal to the volume fractions.

As etching for the LIMI investigations should have suppressed the twin boundaries, the corresponding grain size measurements must be compared to the EBSD results with all twins removed. Surprisingly, the average grain diameters yielded by LIMI measurements are very close to the EBSD values without twin removal (Fig. 11). This means that either the etching procedure did not successfully suppress all of the twins, the threshold value was not chosen correctly or the twin removal routine of the EBSD software did not work reliably. Another source of error for the LIMI measurements, as already mentioned above, might be the influence of the profiles of big deformed grains cut close to the edges, which might also shift the average grain diameter of the deformed grains to lower values.

A good agreement for the grain sizes measured by EBSD and those simulated can be found for strains up to 0.7. But a critical grain size cannot be derived from the measurements. In the calculations, a critical strain of 0.07 and a size of around 15 μm for overcritical recrystallization nuclei were obtained. Since, the strain of 0.11 was actually the smallest strain measured, it cannot be stated reliably whether the corresponding grain size is in conformity with the size of the overcritical recrystallization nuclei. A completely different behavior of the grain size dependence on strain is observed for the two methods at high strains: whereas EBSD gives a continuous rise in the grain size with strain, the simulations show an inflexion point and a subsequent decrease of the grain diameters.

Partitioning between the deformed and recrystallized fractions was performed before twin removal. Removing the twins first and thereafter segmenting the fractions based on grain orientation spread might slightly change the results, because this could give rise to an increased orientation spread in some of the now larger grains. This variation is not, however, possible with the EBSD system in use.

5. Summary

The dynamic recrystallization of the Ni-base alloy Böhler L306 VMR (Alloy 80A) was investigated in a transient state both by optical microscopy (LIMI) and electron backscatter diffraction, and the results were compared to those from simulations.

A sound determination of the recrystallized fraction is generally possible by EBSD, whereas measurements by LIMI and image processing failed at strains higher than around 0.7. EBSD provides additional information about the density and distribution of dislocations.

In the deformed fraction a subgrain structure predominantly close to the grain boundaries can be observed, with the subgrains having approximately the size of the recrystallized grains. The original deformed grains developed a pronounced texture with increasing strain. This texture cannot be observed in the recrystallized fraction.

The recrystallized grains are strongly twinned, with an area fraction of the twinned grains of about 80% for higher strains. The calculated average diameters of the recrystallized grains depend strongly on whether or not the twins have been removed before the grain size calculation started. An increase in the average grain size with increasing strain was only observed if the twins had been removed.

Good agreement was observed between the EBSD measurements and the simulated results, especially for the nucleus density as a function of strain. For both the recrystallized grain sizes and the recrystallized fractions deviations were observed mainly for higher strains.

References

[1] G. Gottstein, Physikalische Grundlagen der Metallkunde, second ed., Springer, Berlin, Heidelberg, 2001.
[2] R.W. Cahn, in: R.W. Cahn, P. Haasen (Eds.), Physical Metallurgy, part 2, third ed., North Holland Physics Publishing, 1983.
[3] T. Sakai, J.J. Jonas, Acta Metal. 32 (2) (1984) 189–209.
[4] F. Montheillet, J. Le Coze, Phys. Status Solidi A 189 (1) (2002) 51–58.
[5] V. Randle, O. Engler, Texture Analysis, Gordon and Breach Science Publishers, 2000.
[6] T.R. McNelley, in: A.J. Schwartz, M. Kumar, B.L. Adams (Eds.), Electron Backscatter Diffraction in Materials Science, Kluwer Academic/Plenum Publishers, 2000.
[7] M. Walter, C. Sommitsch, F. Wedl, S. Kleber, in: P. Portellea (Ed.), Fortschritte in der Metallographie 35, Werkstoff-Informationsges, Frankfurt a. Main, 2004, pp. 245–250.
[8] S. Mitsche, P. Poelt, C. Sommitsch, M. Walter, Proc. Micr. Conf. MC 2003, Microsc. Microanal. 9, Suppl. 3 (2003) 344–345.
[9] S.I. Wright, Proceedings of the 12th International Conference on Textures, 1999, pp. 104–109.
[10] J. Tarasiuk, P.H. Gerber, B. Bacroix, Acta Mater. 50 (2002) 1467–1477.
[11] R. Sandstroem, R. Lagneborg, Acta Metall. 23 (1975) 387–398.
[12] W. Roberts, B. Ahlblom, Acta Metall. 26 (1978) 801–813.
[13] N. Srinivasan, Y.V.R.K. Prasad, Mater. Sci. Technol. 8 (1992) 206–212.
[14] C. Sommitsch, S. Kleber, Mater. Sci. Forum 426–432 (2003) 743–748.
[15] C. Sommitsch, V. Wieser, S. Kleber, J. Mater. Process. 125–126 (2002) 130–137.
[16] C. Zener, TMS-AIME 175 (1949) 175.
[17] J. Cahn, Acta Metall. 10 (1962) 789.

[18] J.P. Thomas, E. Bauchet, C. Dumont, F. Montheillet, in: K.A. Green, T.M. Pollock, H. Harada, T.E. Howson, R.C. Reed, J.J. Schirra, S. Walston (Eds.), Superalloys 2004, TMS (The Minerals, Metals & Materials Society), 2004, pp. 959–968.
[19] T. Sakai, A. Belyakov, H. Miura, in: G. Gottstein, D.A. Molodov (Eds.), Proceedings of the First Joint International Conference on Recrystallisation and Grain Growth, August 2001, RWTH Aachen, Springer, 2001, pp. 669–682.
[20] T. Sakai, in: S. Yue, E. Es-Sadiqi (Eds.), Proceedings of Thermomechanical Processing of Steel—J.J. Jonas Symposium, August 2000, TMS-CIM, Montreal, 2000, pp. 47–62.
[21] F. Montheillet, J. Lepinoux, D. Weygand, E. Rauch, Adv. Eng. Mater. 3 (8) (2001) 587–589.
[22] V. Randle, Scripta Mater. 44 (2001) 2789–2794.
[23] S.I. Wright, R.J. Larsen, J. Microsc. 205 (3) (2002) 245–252.